Journal of Molecular Modeling (2022) 28:354
https://doi.org/10.1007/s00894-022-05341-2

ORIGINAL PAPER

# Reactivity and binding mode of disulfiram, its metabolites, and derivatives in SARS-CoV-2 PL$^{pro}$: insights from computational chemistry studies

**Pablo Andrei Nogara[1,2] · Folorunsho Bright Omage[1] · Gustavo Roni Bolzan[1] · Cássia Pereira Delgado[1] · Laura Orian[3] · João Batista Teixeira Rocha[1]**

Received: 29 May 2022 / Accepted: 28 September 2022


## Abstract

The papain-like protease (PL$^{pro}$) from SARS-CoV-2 is an important target for the development of antivirals against COVID-19. The safe drug disulfiram (DSF) presents antiviral activity inhibiting PL$^{pro}$ in vitro, and it is under clinical trial studies, indicating to be a promising anti-COVID-19 drug. In this work, we aimed to understand the mechanism of PL$^{pro}$ inhibition by DSF and verify if DSF metabolites and derivatives could be potential inhibitors too. Molecular docking, DFT, and ADMET techniques were applied. The carbamoylation of the active site cysteine residue by DSF metabolite (DETC-MeSO) is kinetically and thermodynamically favorable ($\Delta G^{\ddagger} = 3.15$ and $\Delta G = -12.10$ kcal mol$^{-1}$, respectively). Our results strongly suggest that the sulfoxide metabolites from DSF are promising covalent inhibitors of PL$^{pro}$ and should be tested in in vitro and in vivo assays to confirm their antiviral action.

**Keywords** COVID-19 · Organochalcogens · Antiviral compounds · Docking · DFT calculations · Disulfiram

## Introduction

Coronavirus disease 2019 (COVID-19) caused by the severe acute respiratory syndrome coronavirus 2 (SARS-CoV-2) is a critical concern worldwide. The search for an effective antiviral drug to treat COVID-19 is still a challenge. In this sense, the viral protease enzymes are important targets for drug repositioning and new drugs development [1]. The main protease (M$^{pro}$, or 3C-like protease — 3CL$^{pro}$) and papain-like protease (PL$^{pro}$) are essential for viral replication due to their post-translational action on pp1a and pp1ab polyprotein processing. The catalytic dyad and triad from Mpro and PL$^{pro}$, respectively, are responsible for the peptide hydrolase activity, with cysteine (Cys) residues playing a central role in the catalysis, due to the nucleophilic character of the thiolate [2, 3].

Vast effort has been done in the search for SARS-CoV-2 proteases' inhibitors [4–8]. Here, we highlight the organochalcogen drugs ebselen and disulfiram (DSF or Antabus) which have been demonstrated to inhibit the M$^{pro}$ and PL$^{pro}$ from SARS-CoV-2 [9–11] and PL$^{pro}$ from MERS-CoV and SARS-CoV [12, 13]. Disulfiram, which inhibits the mammal aldehyde dehydrogenase (ALDH) enzyme irreversibly, deserves attention because it is a safe and well-studied medicine for alcoholism therapy, with a long duration of action [14–17], as well as a potential drug for HIV latency reversal [18], indicating that it is a good candidate for drug repositioning. DSF prevents SARS-CoV-2 replication in cell-based assays (half-maximal effective concentration, $EC_{50} > 10$ μM) and inhibits PL$^{pro}$ with half-maximal inhibitory concentration ($IC_{50}$) of 6.9–7.5 μM, respectively [9–11]. However, in the presence of reducing thiol molecules such as glutathione

This paper belongs to Topical Collection XXI - Brazilian Symposium of Theoretical Chemistry (SBQT2021)

✉ Pablo Andrei Nogara
pbnogara@gmail.com

✉ João Batista Teixeira Rocha
jbtrocha@yahoo.com.br

[1] Departamento de Bioquímica E Biologia Molecular, Universidade Federal de Santa Maria (UFSM), Av. Roraima 1000, Santa Maria, RS 97105-900, Brazil

[2] Instituto Federal de Educação Ciência E Tecnologia Farroupilha (IFFar), Rua Fabio João Andolhe 1100, Santo Augusto, RS 98590-000, Brazil

[3] Dipartimento Di Scienze Chimiche, Università Degli Studi Di Padova, Via Marzolo 1, 35131 Padua, Italy

Published online: 12 October 2022

(GSH) or dithiothreitol (DTT), the inhibitory effect of DSF is weakened [10], suggesting that GSH and DTT can reduce DSF to diethyldithiocarbamate, which does not inhibit the proteases. Lobo-Galo et al. [19] showed that DSF and some metabolites can bind to the $M^{pro}$ active site interacting with the Cys145 residue. However, little is known about its binding and interactions with the $PL^{pro}$ enzyme.

In this work, we aimed to understand the mechanism of $PL^{pro}$ inhibition by DSF and verify if DSF metabolites and derivatives (Fig. 1) could be potential inhibitors, by applying in silico protocols (molecular docking, density functional theory (DFT) calculations, and ADMET (absorption, distribution, metabolism, excretion, and toxicity) analysis). New acquired data can help in the design of new potential drugs against SARS-CoV-2. Here, each DSF metabolite isomer was studied that could be tested in vitro to confirm their inhibitory potential and antiviral activity.

## Materials and methods

### Disulfiram derivatives

With the aim of finding approved DSF analogs, a search was made on DrugBank [22]. The Thiram and dipentamethylenethiuram disulfide (DPTD) compounds were found as approved drugs (Fig. 1). Thus, they were included in our in silico studies to verify if they might be $PL^{pro}$ inhibitors.

### DFT calculations

Gaussian 16 [23] was used for all density functional theory (DFT) calculations involving reactivity descriptors of DSF and metabolites. The B3LYP hybrid functional was used combined to the Grimme D3 dispersion correction and the Becke-Johnson damping function [24, 25]. All first and second period atoms were described using the 6-311G(d,p) basis set, whereas sulfur atoms were described using Dunning's correlation consistent cc-pVTZ basis set. In the gas phase, all structures were optimized and frequency calculations were used to assess the stationary nature of the geometries before the wavefunction analysis of the reactivity descriptors. This level of theory was applied with success to investigate sulfur reactivity in biological context [26, 27]. The condensed Fukui function [28] was computed using the Hirshfeld charges [29], which were found to have a high overall reactivity prediction performance [30, 31]. ORCA 4.2.1 [32, 33], B3LYP functional, and a triple-quality basis set (def2 TZVP) were used for

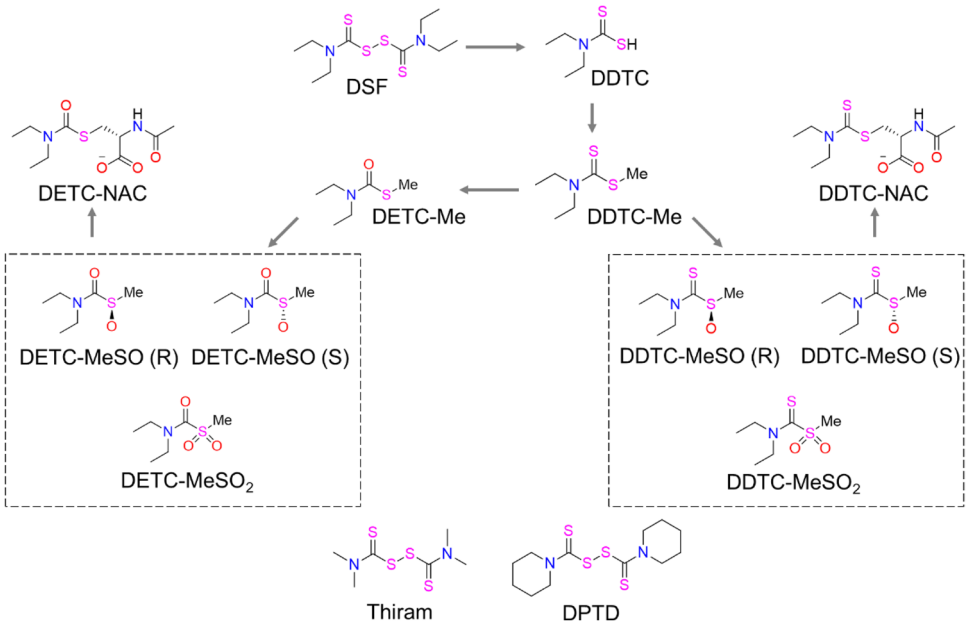


**Fig. 1** Chemical structure of disulfiram (DSF), metabolites, and derivatives. DSF derivatives are shown at the bottom. Disulfiram (DSF); diethyldithiocarbamate (DDTC); S-methyl-N,N-diethyldithiocarbamate (DDTC-Me); S-methyl-N,N-diethylthiocarbamate (DETC-Me); (R) S-methyl-N,N-diethyldithiocarbamate sulfoxide (DDTC-MeSO (R)); (S) S-methyl-N,N-diethyldithiocarbamate sulfoxide (DDTC-MeSO (S)); S-methyl-N,N-diethyldithiocarbamate sulfone (DDTC-$MeSO_2$); diethyldithiocarbamate N-acetylcysteine adduct (DDTC-NAC); (R) S-methyl-N,N-diethylthiocarbamate sulfoxide (DETC-MeSO (R)); (S) S-methyl-N,N-diethylthiocarbamate sulfoxide (DETC-MeSO (S)); S-methyl-N,N-diethylthiocarbamate sulfone (DETC-$MeSO_2$); diethylthiocarbamateN-acetylcysteine adduct (DETC-NAC); dipentamethylenethiuram disulfide (DPTD). For more information about the DSF metabolites, see the references [20, 21]. The active metabolites, which inhibit the ALDH, are highlighted in the boxes

the $S_N2$ mechanism of the reaction between $CH_3S^-$ (Cys model) and the disulfiram (DSF) metabolites DETC-MeSO(S) [26]. To account for dispersion corrections, the Grimme D3 parameterized adjustment to the DFT energy (with Becke-Johnson damping) was used [34]. All structures of intermediate species were found to be local energy minima (no imaginary frequencies) and saddle points (one imaginary frequency) for the transition state (TS). To confirm that the TS was the correct saddle point connecting reactants and products, we calculated the TS's intrinsic reaction coordinate (IRC) defined according to Fukui et al. [35].

### Docking simulations

Docking simulations were carried out according to the literature [36], using the AutoDock Vina [37] with exhaustiveness of 50. The crystallographic structure of $PL^{pro}$ was obtained from the Protein Data Bank (PDB ID: 7JN2). Water, ions, ligands, and other molecules were removed from the X-ray protein structures, and hydrogen was added using the CHIMERA program, followed by 100 steps of energy minimization [38]. Blind docking simulations were applied to the $PL^{pro}$ monomer (coordinates 54.02, 40.34, 11.92 and size 72 × 70 × 46 Å). In addition, with the aim to improve the interactions with the target Cys residues, the grid box was centered on the active site (coordinates 39.64, 30.68, 1.66; size: 20 × 20 × 20 Å) and zinc site (coordinates 82.40 × 26.32 × − 0.62; size: 20 × 20 × 20 Å) because DSF can promote $Zn^{2+}$ ion ejection from $PL^{pro}$ [11].

The ligands' structures were based on their protonation state at physiological pH (Figure S2), where they are mainly in the neutral form, with exception of the N-acetylcysteine (NAC) derivatives (carboxyl moiety is deprotonated) and DDTC. MarvinSketch was used to predict the molecules' protonation state in different pHs (ChemAxon, www.chemaxon.com). Taking into account that the distances between the Cys residues and the DDTC-deprotonated were higher than the protonated one (Figure S3), we decide to present the data with the DDTC neutral in the main text. The tridimensional model of DSF, its metabolites, and derivatives were obtained by gas-phase optimizations carried out at B3LYP-D3(BJ)/6-311G(d,p), cc-pVTZ (see above). Both *R*- and *S*-isomers of the sulfoxides were considered because the sulfur nucleus is a chiral center, which is little explored in docking studies. For each ligand, the 20 best conformers (in terms of binding energies) were grouped in clusters with an RMSD threshold of 2 Å [39]. The best distance (from the most populated cluster) between the S (Cys) atom to S atom (or C = S or C = O groups) was considered as potential sites for the covalent bond formation between the $PL^{pro}$ and organochalcogen ligands, respectively. The analysis and figures were performed using the Discovery Studio Visualizer program [40]. The N–C = S and N–C = O bonds of the ligands were kept rigid during the simulations due to their partial double bond character [41, 42]. The estimate binding sites of $PL^{pro}$ were searched by using DeepSite, a protein-binding site predictor [43].

### ADMET properties

ADMET parameters help us to identify the drugability of molecules. The prediction of the ADMET properties of the ligands was made using pkCSM [44] and SwissADME [45] web freeware servers.

## Results and discussion

### Nucleophilic attack facility

Understanding the chemical reactivity of molecules is essential in drug discovery and the calculation of Fukui functions is a good option for such prediction. In particular, the nucleophilic Fukui function ($f^+$) indicates the susceptibility of different molecular sites to nucleophilic attack [30]. The analysis of the $f^+$ indices of DSF, its metabolites, and derivatives (Table 1) shows that the S atoms of the disulfide bond and the S from the thiocarbonyl moiety are the most favorable sites for the nucleophilic attack, suggesting that the thiolate from Cys residue may attack these moieties. In fact, a covalent adduct with a disulfide bond between half of DSF and the S from Cys residues (thiocarbamoylation) was observed in *Giardia lamblia* carbamate kinase enzyme [46] and recombinant rat liver mitochondrial ALDH (rmALDH) [16]. However, the literature data about the DSF metabolites indicate that the thiolate of Cys attacks the carbon atom of the (thio)carbonyl moieties (carbamoylation) [16, 20, 21]. Despite the highest $f^+$ indices are computed for the S atoms of DSF metabolites, the carbon center from the (thio) carbonyl groups is also reactive and display higher values than the corresponding carbon center in the parent drugs (Table 1). This is a nice result, taking into account that calculations are performed in gas-phase and no environment effects are included.

### Blind docking

To explore the possible binding sites of DSF, its metabolites, and analogs on $PL^{pro}$, blind docking simulations were carried out. The molecules interact in five main binding sites (A–E). Sites A and B present the major number of conformers of DSF, its metabolites, and derivatives (Fig. 2), suggesting a possible allosteric inhibition. Despite the low number of conformers binding to site C, an interaction with a Cys

**Table 1** $f^+$ indices for nucleophilic susceptible sites with DSF, its metabolites, and derivatives

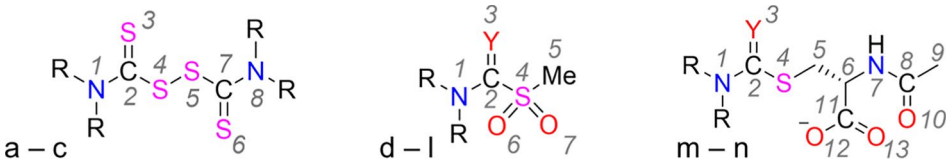


| Molecule | N1 | C2 | S3 | S4 | S5 | S6 | C7 | N8 |
|---|---|---|---|---|---|---|---|---|
| a- DSF | 0.04 | 0.06 | **0.13** | 0.10 | 0.10 | **0.12** | 0.06 | 0.03 |
| b- Thiram | 0.02 | 0.03 | **0.17** | 0.12 | 0.13 | **0.19** | 0.06 | 0.03 |
| c- DPTD | 0.02 | 0.04 | **0.16** | 0.11 | 0.12 | **0.18** | 0.06 | 0.03 |
| | **N1** | **C2** | **S/O3** | **S4** | **C5** | **O6** | **O7** | - |
| d- DDTC | 0.06 | 0.14 | **0.29** | 0.17 | - | - | - | - |
| e- DDTC-Me | 0.05 | 0.14 | **0.26** | 0.14 | 0.03 | - | - | - |
| f- DETC-Me | 0.00 | 0.02 | 0.04 | **0.14** | 0.07 | - | - | - |
| g- DDTC-MeSO (*R*) | 0.07 | 0.12 | **0.26** | 0.09 | 0.04 | 0.06 | - | - |
| h- DDTC-MeSO (*S*) | 0.06 | 012 | **0.27** | 0.10 | 0.04 | 0.06 | - | - |
| i- DDTC-$MeSO_2$ | 0.07 | 0.13 | **0.28** | 0.04 | 0.02 | 0.06 | 0.06 | - |
| j- DETC-MeSO (*R*) | 0.05 | 0.12 | 0.11 | **0.15** | 0.06 | 0.07 | - | - |
| k- DETC-MeSO (*S*) | 0.05 | 0.12 | 0.12 | **0.16** | 0.06 | 0.07 | - | - |
| l- DETC-$MeSO_2$ | 0.05 | **0.15** | **0.15** | 0.07 | 0.03 | 0.07 | 0.07 | - |
| | **N1** | **C2** | **S/O3** | **S4** | **C8** | **C11** | - | - |
| m- DDTC-NAC | 0.05 | 0.13 | **0.22** | 0.12 | 0.02 | 0.01 | - | - |
| n- DETC-NAC | 0.01 | 0.04 | 0.04 | **0.07** | 0.02 | 0.01 | - | - |

Values in bold highlighted the highest $f^+$ indices for each molecule. An atom in a molecule with a positive $f^+$ value is susceptible to nucleophilic attack. Y = O or S

residue (Cys181) occurs, indicating that this residue might be a target, especially for Thiram and DPTD. The analysis with DeepSite corroborates the docking data, and for the sites A, B, C, and D, the scores 0.84, 0.97, 0.53, and 0.99 were obtained, respectively. However, the DeepSite program did not find site E (Glu203, Met206, Met208, and Lys232); conversely, it identified a binding site on the finger domain (between the residues Gln195, Ile222, Thr225, and Lys232). Unfortunately, no molecule interacted here. Next, we studied the interactions of the compounds in the active site and Zn binding site of $PL^{pro}$, due to the presence of critical Cys residues.

## $PL^{pro}$: interactions in the active site

In the catalytic triad of $PL^{pro}$ of SARS-CoV-2, Cys111 acts as a nucleophile by cleaving the peptide bond of pp1a and pp1ab polyprotein, and His272 and Asp286 residues act as an acid–base pair promoting the thiol deprotonation and thus enhancing its nucleophilicity [3, 47]. So, blocking the thiol moiety of Cys111 is a strategy to inhibit the $PL^{pro}$. The predicted binding poses obtained from the docking studies focused on the active site demonstrate that a sulfur atom of the disulfide bond of DSF can interact with the thiol moiety of Cys111 (Fig. 3A and Table 2). These data indicate that the thiocarbamoylation of Cys111 might be possible, as also observed in the *Giardia lamblia* carbamate kinase enzyme [46] and $Ca^{2+}$-bound S100B protein [48]. The DDTC and DDTC-Me metabolites show a similar binding pose and an S•••C = S interaction at 4.9 Å. In contrast, DETC-Me showed an S•••C = O interaction of 4.4 Å (Fig. 3B–D). The dithiocarbamate metabolites DDTC-MeSO (*R*) and DDTC-MeSO (*S*) interact better with Cys111 than DDTC-$MeSO_2$ (Fig. 3E–G), as indicated by the shortest S•••C = S interaction. Among the sulfoxide and sulfone metabolites of DETC-Me (Fig. 3I–K), DETC-MeSO (*S*) presents the best interaction with the PLpro active site, where the oxygen atoms are involved in H-bonds with Cys111, and an S•••C = O interaction at 4.2 Å is also present. This short S•••C = O interaction indicates that the covalent modification of Cys side chain

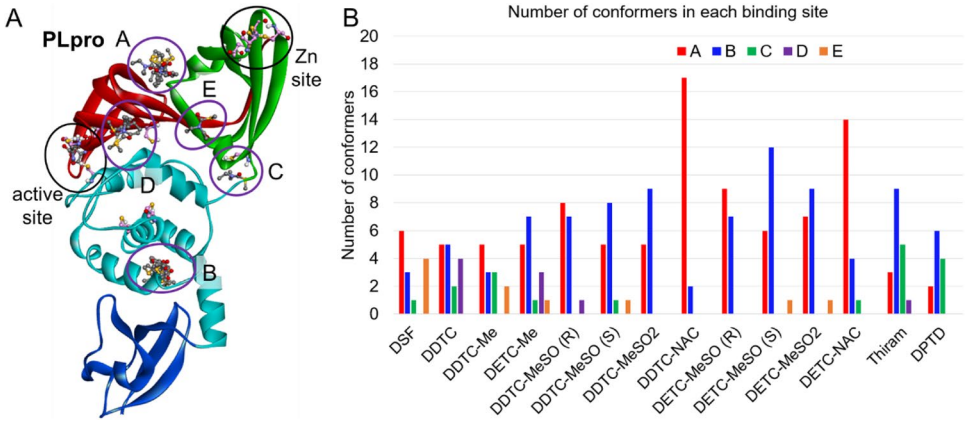


**Fig. 2** Blind docking of $PL^{pro}$. (A) Structure of $PL^{pro}$: the binding sites are represented with purple circles. DETC-Me was used as a representative molecule. The $PL^{pro}$ domains ubiquitin-like, thumb, finger, palm (residues 1–60, 61–178, 179–240, and 241–315, respectively) are shown in blue, cyan, green, and red color, respectively. (B) Number of conformers in the binding sites of $PL^{pro}$

could be possible, as reported by Lipsky et al. [16] in the rmALDH assay.

The N-acetylcysteine metabolites, DDTC-NAC and DETC-NAC, do not show S•••S or S•••C=S/O interactions, but they interact with Cys111 through the carbonyl moiety of the N-acetyl group (Fig. 3H and L). Thiram presents an S•••C=S interaction at 4.9 Å and the DPTD shows an S•••S interaction at 5.4 Å with Cys111 (Fig. 3M, N), suggesting a poorer binding pose and activity than DSF. In addition, we performed the $PL^{pro}$ docking with the active site in the ionic/charged state at physiological pH [49], i.e., the Cys111 deprotonated, His272 protonated, and Asp286 deprotonated. The docking results do not present big changes, with the RMSD ranging from 0.1 to 2.3 Å, between the $PL^{pro}$ docking with the active site neutral and ionic (Table S1 and Figure S1).

It is important to note that the H-bond between the sulfoxide moiety of DDTC-MeSO (*S*), DETC-MeSO (*R*), and DETC-MeSO (*S*) and the amine group of Cys111 is an essential feature for the complexes' stabilization and that it may help the Cys111 nucleophilic attack to these ligands. Despite the least negative predicted binding energies observed here, the structural data help us to better understand the possible mechanism of inhibition of DSF and its metabolites against SARS-CoV-2 $PL^{pro}$. In general, the hydrophobic and van der Waals interactions with Trp106, Asn109, Leu162, and His272, and the H-bonds with Ala107, Ans109, and Cys111 play an important role to stabilize the $PL^{pro}$-ligand complexes. In fact, these residues interact with many inhibitors [50, 51] and they are also involved in the DSF interaction with $PL^{pro}$ from SARS-CoV [12].

## $PL^{pro}$: Zn site interactions

While the active sites of $PL^{pro}$ have only one Cys residue as a target, the Zn site is composed of a Zn(II) ion linked to four Cys residues (Cys189, Cys192, Cys224, and Cys226). This type of Cys-rich motif structure is found in many proteins, such as zinc finger proteins [52]. These small regions of the protein's three-dimensional structure may have important structural and catalytic functions and are a potential molecular target for therapeutic intervention. For this reason, the disruption of protein function via the oxidation of cysteine residues by an organochalcogen at the $PL^{pro}$ Zn binding site deserves to be investigated in more detail. The disruption of the protein may occur through the ejection of zinc ion at the $PL^{pro}$ Zn site of SARS-CoV-2, as mentioned by Sargsyan et al. [11], where the clinically safe drugs ebselen and DSF can covalently bind to cysteine residues, thus forming a covalent adduct.

The binding poses obtained from the docking studies focused on the $PL^{pro}$ Zn site demonstrate that the sulfur atom of the DSF disulfide bond can interact with the thiolate group of Cys224 (Fig. 4A and Table 2). The DDTC, DDTC-Me, and DETC-Me metabolites also interact with the Cys224 through S•••C=S/O interaction, with a small binding pose difference (Fig. 4B–D). The dithiocarbamate sulfoxide metabolites DDTC-MeSO (*R*), DDTC-MeSO (*S*), and DDTC-$MeSO_2$ interact with the Cys224 through S•••C=S interaction (Fig. 4E–G), while the thiocarbamates DETC-MeSO (*R*), DETC-MeSO (*S*), and DETC-$MeSO_2$ bind through S•••C=O interaction (Fig. 4I–K). As observed in the active site, the DETC-MeSO (*S*) has a better interaction with the Zn site, where oxygen atoms form H-bonds with Thr225, and there is also an S•••C=O interaction at 3.6 Å. The metabolites from N-acetylcysteine, DDTC-NAC and DETC-NAC, like observed in the active site, do not present S•••S or S•••C=S/O interactions. They interact with Cys224 with the carbonyl portion of the N-acetyl group (Fig. 4H–L). The studied derivatives show similar behavior to DSF, especially Thiram. Both Thiram and DPTD show S•••C=S and S•••S interactions (Fig. 4N, O); however, the shorter S•••S distance (3.9 Å) of the Thiram derivative suggests a better binding pose and activity than DPTD. In this

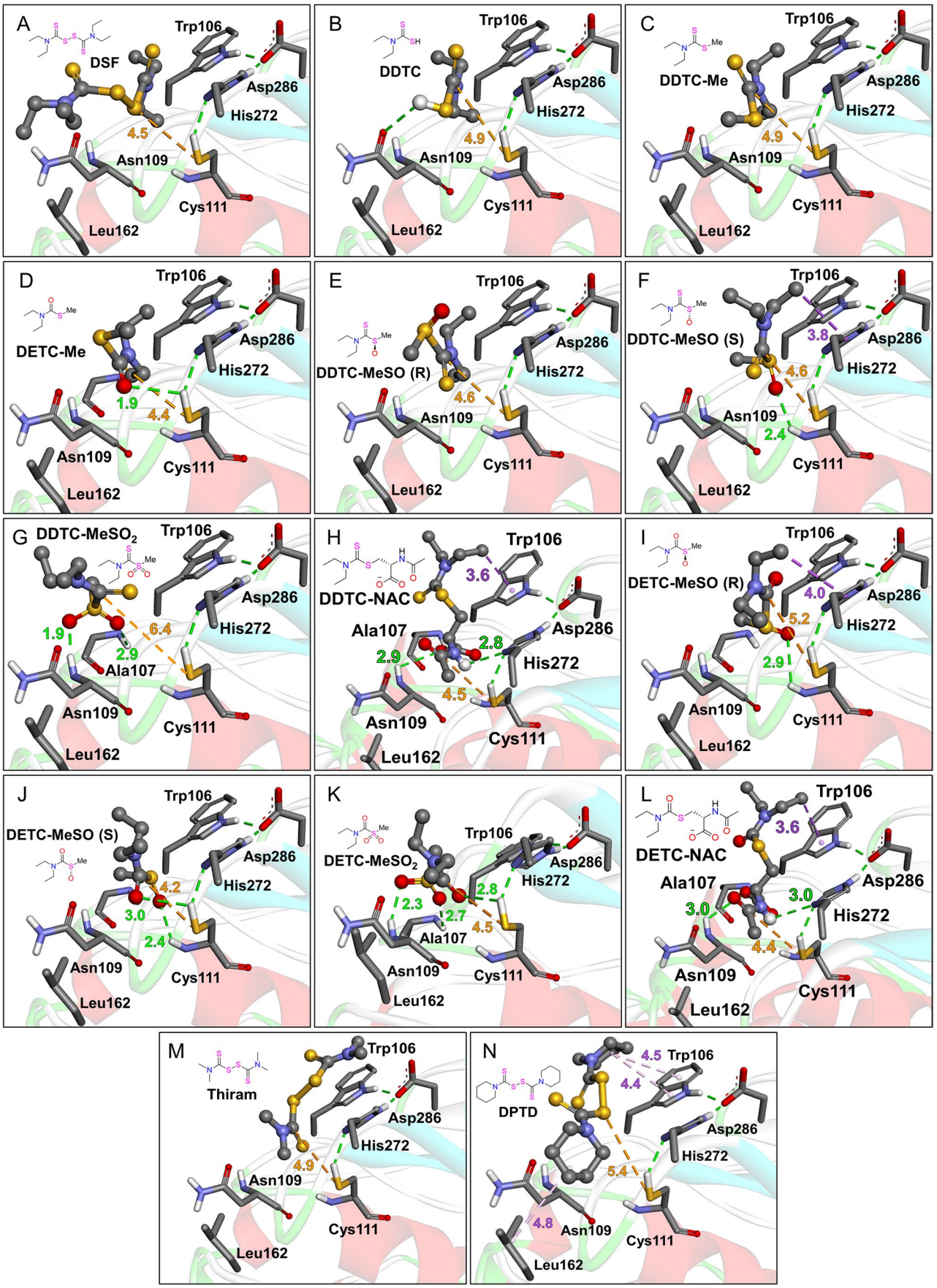
A
DSF
Trp106
Asp286
His272
4.5
Asn109
Cys111
Leu162
B
DDTC
Trp106
Asp286
His272
4.9
Asn109
Cys111
Leu162
C
DDTC-Me
Trp106
Asp286
His272
4.9
Asn109
Cys111
Leu162
D
DETC-Me
Trp106
Asp286
His272
1.9
4.4
Asn109
Cys111
Leu162
E
DDTC-MeSO (R)
Trp106
Asp286
His272
4.6
Asn109
Cys111
Leu162
F
DDTC-MeSO (S)
Trp106
3.8
Asp286
4.6
His272
Asn109
2.4
Cys111
Leu162
G
DDTC-MeSO2
Trp106
Asp286
1.9
6.4
His272
2.9
Ala107
Asn109
Cys111
Leu162
H
DDTC-NAC
Trp106
3.6
Ala107
Asp286
2.8
2.9
His272
4.5
Asn109
Cys111
Leu162
I
DETC-MeSO (R)
Trp106
4.0
Asp286
5.2
His272
2.9
Asn109
Cys111
Leu162
J
DETC-MeSO (S)
Trp106
Asp286
4.2
His272
3.0
2.4
Asn109
Cys111
Leu162
K
DETC-MeSO2
Trp106
Asp286
His272
2.8
2.3
2.7
4.5
Ala107
Asn109
Cys111
Leu162
L
DETC-NAC
Trp106
3.6
Ala107
Asp286
3.0
3.0
His272
4.4
Asn109
Cys111
Leu162
M
Thiram
Trp106
Asp286
His272
4.9
Asn109
Cys111
Leu162
N
DPTD
4.5
Trp106
4.4
Asp286
His272
5.4
4.8
Asn109
Cys111
Leu162

◂**Fig. 3** $PL^{pro}$ docking with DSF, its metabolites, and derivatives. H-bonds, hydrophobic, and S···S (or S···C = O/S) interactions are represented by green, purple, and orange dashed lines, respectively. The distances are in Å

sense, DSF analogues should be better studied as possible $PL^{pro}$ inhibitors.

It is important to note that the H-bonds with a Gln195 and Thr225 could help to stabilize the $PL^{pro}$ Zn-ligand complexes, and may be of great value in the mechanism of inhibition of this site, promoting the possible ejection of the Zn ion, after the nucleophilic attack of Cys224 (which was found to be the target Cys residue), as reported in a previous study [11].

## Energetics of thiolate attack to DSF and DETC-MeSO (S)

As observed by the docking study, the disulfide (S–S) bond of DSF and the carbamoyl moiety of DETC-MeSO (S) metabolite are Cys' warheads. Thus, to understand the potential covalent inhibition, DFT calculations were carried out using as a model the nucleophile methylthiolate ($CH_3S^-$) (a Cys' lateral chain model), as done in other theoretical studies [26, 36]. The DSF and DETC-MeSO (S) can form adducts with the Cys' lateral chain, in an energetically favorable exergonic reaction ($\Delta G = -26.9$ and $-12.1$ kcal $mol^{-1}$, respectively) (Fig. 5). In fact, theoretical studies indicate that this reaction is thermodynamically favored [26, 53].

Focusing on the potential inhibition by DETC-MeSO (S), it was verified that $CH_3S^-$ proceeds via a concerted nucleophilic attack mechanism on the carbonyl (C = O) group of DETC-MeSO (S), which has been located on the potential energy surface (PES) and confirmed by an intrinsic reaction coordinate (IRC) calculation. This is consistent with the earlier mechanistic analysis reported by our group [36, 54]. The reaction starts with the formation of a reactant complex (RC), in which the $CH_3S^-$ (nucleophile) coordinates to the carbonyl-carbon group of DETC-MeSO (S) (substrate) at 3.14 Å. In the gas phase, the reactant complexes are stabilized by 13.20 kcal $mol^{-1}$ with respect to isolated reactants. At the transition state (TS), the overall energy barrier is 3.20 kcal $mol^{-1}$ relative to the RC, and the length of the S•••C = O bond of $CH_3S^-$ (nucleophile, 2.01 Å) gets progressively shorter, while the length of the S•••C = O bond of DETC-MeSO (S) (leaving group, 2.25 Å) gets longer and eventually breaks completely, releasing the methylsulfenate anion ($CH_3SO^-$). The TS was found to have only one imaginary frequency, proving the structure's rationality. Taking all together, the docking simulations and DFT calculations highlight that the S•••C = O (thiol/thiolate••• carbamoyl) interaction and the consequent Cys' nucleophilic attack on the carbamoyl moiety of DETC-MeSO (S) are a key step in the enzyme inhibition mechanism, and it is energetically favorable, suggesting that DSF and metabolites are good Cys' blocking agents due its covalent modification.

**Table 2** Predicted binding free energies ($\Delta G$, kcal•$mol^{-1}$) between $PL^{pro}$ and DSF, its metabolites, and derivatives

| | active site | | | Zn site | | |
|---|---|---|---|---|---|---|
| **Molecule** | **ΔG** | **$E^+$···$S^a$** | **$E^+$** | **ΔG** | **$E^+$···$S^b$** | **$E^+$** |
| DSF | -2.9 | 4.5 | S–S | -3.2 | 4.0 | S–S |
| DDTC | -2.5 | 4.9 | C=S | -2.1 | 5.1 | C=S |
| DDTC-Me | -2.7 | 4.9 | C=S | -2.4 | 4.5 | C=S |
| DETC-Me | -2.8 | 4.4 | C=O | -2.9 | 3.8 | C=O |
| DDTC-MeSO (*R*) | -2.8 | 4.6 | C=S | -2.9 | 4.3 | C=S |
| DDTC-MeSO (*S*) | -3.0 | 4.6 | C=S | -2.7 | 4.1 | C=S |
| DDTC-$MeSO_2$ | -2.7 | 6.4 | C=S | -3.0 | 4.3 | C=S |
| DDTC-NAC | -4.1 | 4.5 | C=O' | -3.7 | 4.3 | C=O' |
| DETC-MeSO (*R*) | -3.0 | 5.2 | C=O | -3.2 | 4.0 | C=O |
| DETC-MeSO (*S*) | -3.1 | 4.2 | C=O | -3.4 | 3.6 | C=O |
| DETC-$MeSO_2$ | -2.8 | 4.5 | C=O | -2.8 | 4.5 | C=O |
| DETC-NAC | -4.1 | 4.4 | C=O' | -3.7 | 4.4 | C=O' |
| Thiram | -3.1 | 4.9 | C=S | -3.4 | 3.9 | S–S |
| DPTD | -3.8 | 5.4 | S–S | -4.2 | 4.5 | S–S |

$E^+$, electrophile group of the ligand, which can be S, C = O, C = S, or the acetyl group (C = O′). The first atom in the column is the electrophilic center of the ligands. Distances (in Å) from the thiol of [a]Cys111 and [b]Cys224 to the $E^+$; green, yellow, and red colors indicate a favorable, intermediate, and less favorable interaction, respectively.

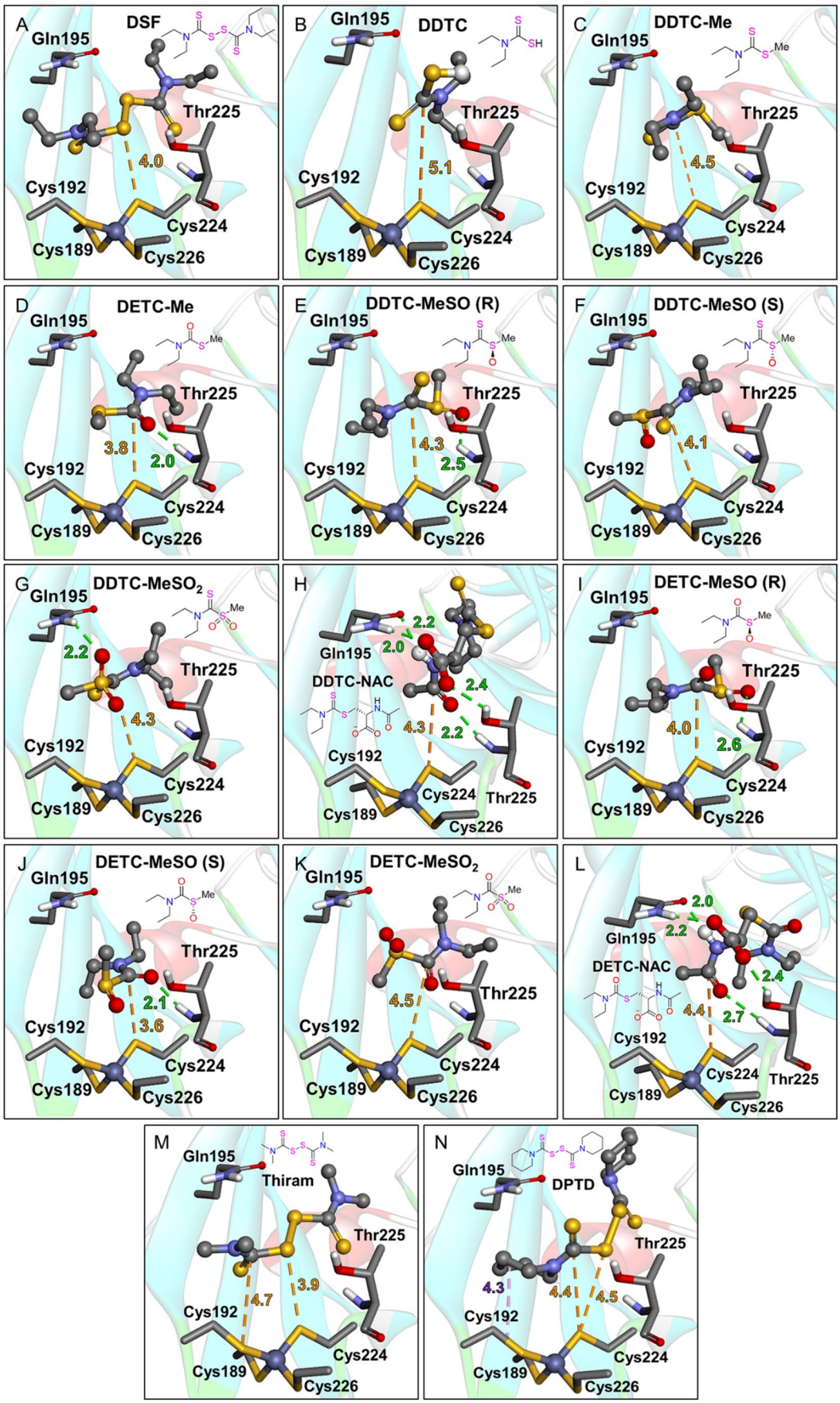
A
DSF
Gln195
Thr225
4.0
Cys192
Cys224
Cys189
Cys226
B
Gln195
DDTC
Thr225
5.1
Cys192
Cys224
Cys189
Cys226
C
DDTC-Me
Gln195
Thr225
4.5
Cys192
Cys224
Cys189
Cys226
D
DETC-Me
Gln195
Thr225
3.8
2.0
Cys192
Cys224
Cys189
Cys226
E
DDTC-MeSO (R)
Gln195
Thr225
4.3
2.5
Cys192
Cys224
Cys189
Cys226
F
DDTC-MeSO (S)
Gln195
Thr225
4.1
Cys192
Cys224
Cys189
Cys226
G
DDTC-MeSO2
Gln195
2.2
Thr225
4.3
Cys192
Cys224
Cys189
Cys226
H
Gln195
2.2
2.0
DDTC-NAC
2.4
4.3
2.2
Cys192
Cys224
Thr225
Cys189
Cys226
I
DETC-MeSO (R)
Gln195
Thr225
4.0
2.6
Cys192
Cys224
Cys189
Cys226
J
DETC-MeSO (S)
Gln195
Thr225
2.1
3.6
Cys192
Cys224
Cys189
Cys226
K
DETC-MeSO2
Gln195
4.5
Thr225
Cys192
Cys224
Cys189
Cys226
L
2.0
Gln195
2.2
DETC-NAC
2.4
4.4
2.7
Cys192
Cys224
Thr225
Cys189
Cys226
M
Gln195
Thiram
Thr225
3.9
4.7
Cys192
Cys224
Cys189
Cys226
N
Gln195
DPTD
Thr225
4.3
4.4
4.5
Cys192
Cys224
Cys189
Cys226

◂**Fig. 4** $PL^{pro}$ Zn site docking with DSF, its metabolites, and derivatives. H-bonds, hydrophobic, and S···S (or S···C=O/S) interactions are represented by green, purple, and orange dashed lines, respectively. The distances are in Å

## ADMET analysis

Prediction of absorption, distribution, metabolism, excretion, and toxicity (ADMET) properties of molecules is essential in drug discovery, giving important information about the drug likeness [44]. For example, the Lipinski's rule of five (molecular weight < 500; number of H-bond donors < 5; number of H-bond acceptors < 10; log*P* < 5) plays an important role in the screening of drugs with pharmacological activity [55]. For these reasons, we have investigated the ADMET features of DETC-MeSO (S) because it demonstrated to be a potential $PL^{pro}$ inhibitor, and compared it to DSF and DDTC-MeSO (S) metabolite. According to Table S2, DSF, DETC-MeSO, and DDTC-MeSO follow Lipinski rules, and they are predicted to have good water solubility, with high Caco-2 permeability and intestinal absorption, and low skin permeability. The metabolites appear to be more hydrophilic than the DSF. Only DSF and DDTC-MeSO showed to be P-glycoprotein substrates. Regarding the distribution properties, the volume of distribution (VDss), which represents if the drug is preferably contained in tissues rather than in plasma, and the unbound fraction suggest an uniform distribution. The blood–brain barrier (BBB) and central nervous system (CNS) permeability imply a moderate distribution to the brain. DETC-MeSO and DDTC-MeSO do not appear to be substrates or inhibitors of hepatic cytochrome P450 isoenzymes (an essential system for drug metabolism in the liver), while DSF might be an inhibitor. The drug excretion prediction indicates that they are not substrates of the organic cation transporter 2 (OCT2), a renal uptake transporter that plays an important role in the disposition and renal clearance of xenobiotics. With exception of the skin sensitization (allergic contact dermatitis) tests, the toxicity assays suggest that the molecules are not toxic. In fact, the DSF lethal dosage ($LD_{50}$) in rats is 8.6 g/kg [56]. In addition, the drug likeness (Table S3), analyzed by five different rule-based filters (Lipinski, Ghose, Veber, Egan, and Muegge), suggests that the compounds are good oral drug candidates [45]. In short, the predicted ADMET properties indicate that DSF, DETC-MeSO, and DDTC-MeSO present good water solubility and absorption, moderate distribution, poor metabolism and excretion, and moderate toxicity. These data are essential in drug design, which can effectively be a guide and lead to a reduction of failures in clinical trials [44]. The replacement of S (in DDTC-MeSO) to O atom (in DETC-MeSO) has a low effect on the predicted ADMET. However, it could have an influence on the molecule reactivity; since O is more electronegative than the S, the DETC-MeSO could be a better electrophile than DDTC-MeSO and be an important thiol target.

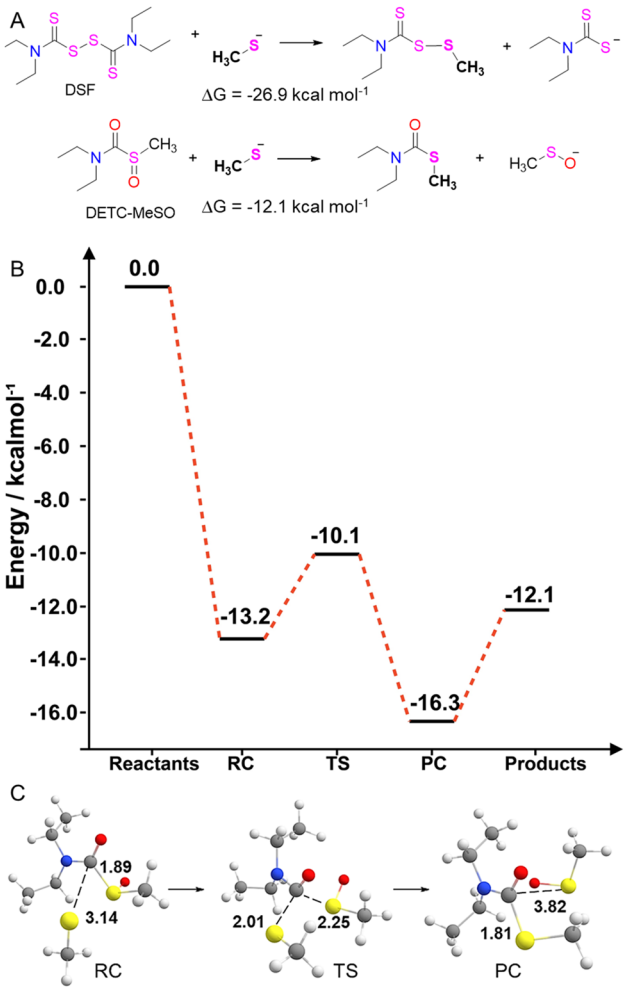


**Fig. 5** (A) Proposed reaction between $CH_3S^-$ (Cys model) and DSF and DETC-MeSO (S). (B) Gas phase energy profile for the reaction for DETC-MeSO (S), and (C) optimized molecular structures of reactant complex (RC), transition state (TS), and product complex (PC). The calculated Gibbs energies are in kcal $mol^{-1}$ and are relative to the energy of the separated reactants. The distances are in Å. Level of theory B3LYP-D3(BJ)/TZVP

## Conclusions

The data here presented suggest that the DSF and metabolites are $PL^{pro}$ inhibitors, which is consistent with the outcomes of previous studies [9–11], besides helping to understand its molecular mechanism of action at the molecular level. Specifically, the sulfoxides metabolite DETC-MeSO (S) show a satisfactory interaction with the thiol group of Cys111 of $PL^{pro}$, suggesting that the inhibition may be covalent, as observed for the ALDH [16, 20, 21], hexokinase [57], and glutathione S-transferase enzymes [58].

We have presented a systematic quantum chemical analysis of the mechanism and energetics of the reactions between

$CH_3S^-$ and a DETC-MeSO (S) using DFT. In vacuo, this reaction proceeds via an $S_N2$ mechanism, and it is kinetically and thermodynamically favorable. Our data suggest a great advantage of DSF because its metabolites are still active and can have pharmacological action. In this way, the use of DSF, its metabolites and derivatives, may be an option in the search for antivirals against COVID-19. Furthermore, DSF was able to block neutrophil extracellular traps (NET) formation and protect rodents against lung injury and SARS-CoV-2 infection [59]. Currently, two clinical trials have been approved to evaluate the effects of DSF in patients with COVID-19 (NCT04594343, NCT04485130), and recent studies suggest that patients undergoing DSF treatment had a reduced COVID-19 infection rate and fewer symptoms than those untreated [60, 61]. Taken as a whole, these data strongly suggest that DSF and active metabolites are important molecules, due to their disulfide and carbamoyl moieties, and should be tested in in vitro and in vivo trials to confirm the inhibitory and pharmacological potential against SARS-CoV-2.

**Supplementary Information** The online version contains supplementary material available at https://doi.org/10.1007/s00894-022-05341-2.

**Author contribution** All authors have read and agreed to the published version of the manuscript. Conceptualization, supervision, methodology, validation, and project administration: P.A.N., L.O., and J.B.T.R. Conceptualization, formal analysis, investigation, and data curation: P.A.N., F.B.O., G.R.B., and C.P.D. Formal analysis and writing — original draft preparation: P.A.N., F.B.O., G.R.B., and C.P.D. Writing — review and editing: P.A.N., L.O., and J.B.T.R.

**Funding** The authors would like to thank the financial support by Coordination for Improvement of Higher Education Personnel CAPES/ PROEX (n° 23038.005848/2018–31; n°0737/2018). J.B.T.R., P.A.N., G.R.B., and C.P.D. were funded by CAPES (Edital 09–88887.505377/2020–00; 88887.511828/2020–00; 88887.512045/2020–00; 88887.512885/2020–00); F.B.O. was funded by CAPES (Edital 88887.354370/2019–00). L.O. was funded by Università degli Studi di Padova, thanks to the P-DiSC (BIRD2018-UNIPD) project MAD$^3$S (Modeling Antioxidant Drugs: Design and Development of Computer-Aided Molecular Systems).

**Data availability** The datasets generated during and/or analyzed during the current study are available in the Supporting Information section.

## Declarations

**Competing interests** The authors declare no competing interests.

## References

1. Amin SA, Banerjee S, Ghosh K et al (2021) Protease targeted COVID-19 drug discovery and its challenges: insight into viral main protease (Mpro) and papain-like protease (PLpro) inhibitors. Bioorganic Med Chem 29:115860. https://doi.org/10.1016/j.bmc.2020.115860
2. Francés-Monerris A, Hognon C, Miclot T et al (2020) Molecular basis of SARS-CoV-2 infection and rational design of potential antiviral agents: modeling and simulation approaches. J Proteome Res 19:4291–4315. https://doi.org/10.1021/acs.jproteome.0c00779
3. Anirudhan V, Lee H, Cheng H et al (2021) Targeting SARS-CoV-2 viral proteases as a therapeutic strategy to treat COVID-19. J Med Virol 93:2722–2734. https://doi.org/10.1002/jmv.26814
4. Choi I, Park Y, Ryu IY et al (2021) In silico and in vitro insights into tyrosinase inhibitors with a 2-thioxooxazoline-4-one template. Comput Struct Biotechnol J 19:37–50. https://doi.org/10.1016/j.csbj.2020.12.001
5. Mangiavacchi F, Botwina P, Menichetti E et al (2021) Selenofunctionalization of quercetin improves the non-covalent inhibition of M pro and its antiviral activity in cells against SARS-CoV-2. Int J Mol Sci 22:7048. https://doi.org/10.3390/ijms22137048
6. Farhat N, Khan AU (2021) Repurposing drug molecule against SARS-Cov-2 (COVID-19) through molecular docking and dynamics: a quick approach to pick FDA-approved drugs. J Mol Model 27:312. https://doi.org/10.1007/s00894-021-04923-w
7. Paul D, Basu D, Ghosh Dastidar S (2021) Multi-conformation representation of Mpro identifies promising candidates for drug repurposing against COVID-19. J Mol Model 27:128. https://doi.org/10.1007/s00894-021-04732-1
8. Cavasotto CN, Di Filippo JI (2021) In silico drug repurposing for COVID-19: targeting SARS-CoV-2 proteins through docking and consensus ranking. Mol Inform 40:2000115. https://doi.org/10.1002/minf.202000115
9. Jin Z, Du X, Xu Y et al (2020) Structure of Mpro from SARS-CoV-2 and discovery of its inhibitors. Nature 582:289–293. https://doi.org/10.1038/s41586-020-2223-y
10. Ma C, Hu Y, Townsend JA et al (2020) Ebselen, disulfiram, carmofur, PX-12, tideglusib, and shikonin are nonspecific promiscuous SARS-CoV-2 main protease inhibitors. ACS Pharmacol Transl Sci 3:1265–1277. https://doi.org/10.1021/acsptsci.0c00130
11. Sargsyan K, Lin CC, Chen T et al (2020) Multi-targeting of functional cysteines in multiple conserved SARS-CoV-2 domains by clinically safe Zn-ejectors. Chem Sci 11:9904–9909. https://doi.org/10.1039/d0sc02646h
12. Lin MH, Moses DC, Hsieh CH et al (2018) Disulfiram can inhibit MERS and SARS coronavirus papain-like proteases via different modes. Antiviral Res 150:155–163. https://doi.org/10.1016/j.antiviral.2017.12.015
13. Tomczak EW, Tomczak JM, Talma M (2021) Identification of ebselen and its analogues as potent covalent inhibitors of papain-like protease from SARS-CoV-2. Sci Rep 11:3640. https://doi.org/10.1038/s41598-021-83229-6
14. Johansson B (1992) A review of the pharmacokinetics and pharmacodynamics of disulfiram and its metabolites. Acta Psychiatr Scand 86:15–26. https://doi.org/10.1111/j.1600-0447.1992.tb03310.x
15. Batalha PN, Forezi LSM, Lima CGS et al (2021) Drug repurposing for the treatment of COVID-19: pharmacological aspects and synthetic approaches. Bioorg Chem 106:104488. https://doi.org/10.1016/j.bioorg.2020.104488
16. Lipsky JJ, Shen ML, Naylor S (2001) Overview - In vitro inhibition of aldehyde dehydrogenase by disulfiram and metabolites. Chem Biol Interact 130–132:81–91. https://doi.org/10.1016/S0009-2797(00)00224-6
17. Quistad GB, Sparks SE, Casida JE (1994) Aldehyde dehydrogenase of mice inhibited by thiocarbamate herbicides. Life Sci 55:1537–1544. https://doi.org/10.1016/0024-3205(94)00314-9

18. Elliott JH, McMahon JH, Chang CC et al (2015) Short-term administration of disulfiram for reversal of latent HIV infection: a phase 2 dose-escalation study. Lancet HIV 2:e520–e529. https://doi.org/10.1016/S2352-3018(15)00226-X
19. Lobo-Galo N, Terrazas-López M, Martínez-Martínez A, Díaz-Sánchez ÁG (2021) FDA-approved thiol-reacting drugs that potentially bind into the SARS-CoV-2 main protease, essential for viral replication. J Biomol Struct Dyn 39:3419–3427. https://doi.org/10.1080/07391102.2020.1764393
20. Hu P, Jin L, Baillie TA (1997) Studies on the metabolic activation of disulfiram in rat. Evidence for electrophilic S-oxygenated metabolites as inhibitors of aldehyde dehydrogenase and precursors of urinary N-acetylcysteine conjugates. J Pharmacol Exp Ther 281:611–617
21. Koppaka V, Thompson DC, Chen Y et al (2012) Aldehyde dehydrogenase inhibitors: a comprehensive review of the pharmacology, mechanism of action, substrate specificity, and clinical application. Pharmacol Rev 64:520–539. https://doi.org/10.1124/pr.111.005538
22. Wishart DS, Feunang YD, Guo AC et al (2018) DrugBank 5.0: a major update to the DrugBank database for 2018. Nucleic Acids Res 46:D1074–D1082. https://doi.org/10.1093/nar/gkx1037
23. Frisch MJ, Trucks GW, Schlegel HB et al (2016) Gaussian 16 (Revision A.03). Gaussian Inc., Wallingford
24. Grimme S (2011) Density functional theory with London dispersion corrections. WIREs Comput Mol Sci 1:211–228. https://doi.org/10.1002/wcms.30
25. Becke AD, Johnson ER (2005) A density-functional model of the dispersion interaction. J Chem Phys 123:154101. https://doi.org/10.1063/1.2065267
26. Bortoli M, Wolters LP, Orian L, Bickelhaupt FM (2016) Addition-elimination or nucleophilic substitution? Understanding the energy profiles for the reaction of chalcogenolates with dichalcogenides. J Chem Theory Comput 12:2752–2761. https://doi.org/10.1021/acs.jctc.6b00253
27 DallaTiezza M, Bickelhaupt FM, Flohé L et al (2020) A dual attack on the peroxide bond. The common principle of peroxidatic cysteine or selenocysteine residues. Redox Biol 34:101540. https://doi.org/10.1016/j.redox.2020.101540
28. Ayers PW, Parr RG (2000) Variational principles for describing chemical reactions: the Fukui function and chemical hardness revisited. J Am Chem Soc 122:2010–2018. https://doi.org/10.1021/ja9924039
29. Hirshfeld FL (1977) Bonded-atom fragments for describing molecular charge densities. Theor Chim Acta 44:129–138. https://doi.org/10.1007/BF00549096
30. Wang B, Rong C, Chattaraj PK, Liu S (2019) A comparative study to predict regioselectivity, electrophilicity and nucleophilicity with Fukui function and Hirshfeld charge. Theor Chem Acc 138:124. https://doi.org/10.1007/s00214-019-2515-1
31. Liu S (2015) Quantifying reactivity for electrophilic aromatic substitution reactions with hirshfeld charge. J Phys Chem A 119:3107–3111. https://doi.org/10.1021/acs.jpca.5b00443
32 Neese F (2018) Software update: the ORCA program system, version 40. WIREs Comput Mol Sci 8:e1327. https://doi.org/10.1002/wcms.1327
33. Neese F, Wennmohs F, Becker U, Riplinger C (2020) The ORCA quantum chemistry program package. J Chem Phys 152:224108. https://doi.org/10.1063/5.0004608
34. Grimme S, Antony J, Ehrlich S, Krieg H (2010) A consistent and accurate ab initio parametrization of density functional dispersion correction (DFT-D) for the 94 elements H-Pu. J Chem Phys 132:154104. https://doi.org/10.1063/1.3382344
35. Fukui K, Kato S, Fujimoto H (1975) Constituent analysis of the potential gradient along a reaction coordinate. Method and an application to CH4+ T reaction. J Am Chem Soc 97:1–7. https://doi.org/10.1021/JA00834A001/ASSET/JA00834A001.FP.PNG_V03
36. Nogara PA, Omage FB, Bolzan GR et al (2021) In silico studies on the interaction between Mpro and PLpro from SARS-CoV-2 and ebselen, its metabolites and derivatives. Mol Inform 40:2100028. https://doi.org/10.1002/minf.202100028
37. Trott O, Olson AJ (2010) AutoDock Vina: improving the speed and accuracy of docking with a new scoring function, efficient optimization, and multithreading. J Comput Chem 31:455–461. https://doi.org/10.1002/jcc.21334
38. Pettersen EF, Goddard TD, Huang CC et al (2004) UCSF Chimera - a visualization system for exploratory research and analysis. J Comput Chem 25:1605–1612. https://doi.org/10.1002/jcc.20084
39. Chang MW, Ayeni C, Breuer S, Torbett BE (2010) Virtual screening for HIV protease inhibitors: a comparison of AutoDock 4 and Vina. PLoS ONE 5:1–9. https://doi.org/10.1371/journal.pone.0011955
40. Biovia DS, Berman HM, Westbrook J, Feng Z et al (2017) Dassault systèmes BIOVIA, San Diego
41. Hameed A, Shafiq Z, Yaqub M et al (2015) Robustness of a thioamide {···H-N-C=S}2 synthon: synthesis and the effect of substituents on the formation of layered to cage-like supramolecular networks in coumarin-thiosemicarbazone hybrids. New J Chem 39:6052–6061. https://doi.org/10.1039/c5nj00734h
42. Sandberg T, Rosenholm J, Hotokka M (2008) The molecular structure of disulfiram and its complexation with silica. A quantum chemical study. J Mol Struct THEOCHEM 861:57–61. https://doi.org/10.1016/j.theochem.2008.04.007
43. Jiménez J, Doerr S, Martínez-Rosell G et al (2017) DeepSite: protein-binding site predictor using 3D-convolutional neural networks. Bioinformatics 33:3036–3042. https://doi.org/10.1093/bioinformatics/btx350
44. Pires DEV, Blundell TL, Ascher DB (2015) pkCSM: predicting small-molecule pharmacokinetic and toxicity properties using graph-based signatures. J Med Chem 58:4066–4072. https://doi.org/10.1021/acs.jmedchem.5b00104
45. Daina A, Michielin O, Zoete V (2017) SwissADME: a free web tool to evaluate pharmacokinetics, drug-likeness and medicinal chemistry friendliness of small molecules. Sci Rep 7:42717. https://doi.org/10.1038/srep42717
46. Galkin A, Kulakova L, Lim K et al (2014) Structural basis for inactivation of Giardia lamblia carbamate kinase by disulfiram. J Biol Chem 289:10502–10509. https://doi.org/10.1074/jbc.M114.553123
47. Ismail MI, Ragab HM, Bekhit AA, Ibrahim TM (2021) Targeting multiple conformations of SARS-CoV2 Papain-like protease for drug repositioning: an in-silico study. Comput Biol Med 131:104295. https://doi.org/10.1016/j.compbiomed.2021.104295
48. Cavalier MC, Pierce AD, Wilder PT et al (2014) Covalent small molecule inhibitors of Ca2+ -bound S100B. Biochemistry 53:6628–6640. https://doi.org/10.1021/bi5005552
49. Henderson JA, Verma N, Harris RC et al (2020) Assessment of proton-coupled conformational dynamics of SARS and MERS coronavirus papain-like proteases: implication for designing broad-spectrum antiviral inhibitors. J Chem Phys 153:115101. https://doi.org/10.1063/5.0020458
50 Rut W, Lv Z, Zmudzinski M et al (2020) Activity profiling and crystal structures of inhibitor-bound SARS-CoV-2 papain-like protease: a framework for anti–COVID-19 drug design. Sci Adv 6:eabd4596. https://doi.org/10.1126/sciadv.abd4596
51. Li D, Luan J, Zhang L (2021) Molecular docking of potential SARS-CoV-2 papain-like protease inhibitors. Biochem Biophys Res Commun 538:72–79. https://doi.org/10.1016/j.bbrc.2020.11.083

52. Cassandri M, Smirnov A, Novelli F et al (2017) Zinc-finger proteins in health and disease. Cell Death Discov 3:17071. https://doi.org/10.1038/cddiscovery.2017.71
53. Madabeni A, Nogara PA, Omage FB et al (2021) Mechanistic insight into SARS-CoV-2 Mpro inhibition by organoselenides: the ebselen case study. Appl Sci 11:6291. https://doi.org/10.3390/app11146291
54. Nogara PA, Madabeni A, Bortoli M et al (2021) Methylmercury can facilitate the formation of dehydroalanine in selenoenzymes: insight from DFT molecular modeling. Chem Res Toxicol 34:1655–1663. https://doi.org/10.1021/acs.chemrestox.1c00073
55. Lipinski CA, Lombardo F, Dominy BW, Feeney PJ (1997) Experimental and computational approaches to estimate solubility and permeability in drug discovery and development settings. Adv Drug Deliv Rev 23:3–25. https://doi.org/10.1016/S0169-409X(96)00423-1
56. Meraz-Torres F, Plöger S, Garbe C et al (2020) Disulfiram as a therapeutic agent for metastatic malignant melanoma - old myth or new logos? Cancers (Basel) 12:1–20. https://doi.org/10.3390/cancers12123538
57. Strömme JH (1963) Inhibition of hexokinase by disulfiram and dlethyldithiocarbamate. Biochem Pharmacol 12:157–166. https://doi.org/10.1016/0006-2952(63)90180-1
58. Ploemen J-PHTM, van Iersel MLPS, Wormhoudt LW et al (1996) In vitro inhibition of rat and human glutathione S-transferase isoenzymes by disulfiram and diethyldithiocarbamate. Biochem Pharmacol 52:197–204. https://doi.org/10.1016/0006-2952(96)00142-6
59. Adrover JM, Carrau L, Daßler-plenker J et al (2022) Disulfiram inhibits neutrophil extracellular trap formation and protects rodents during acute lung injury and SARS-CoV-2 infection. JCI Insight 1:e157342. https://doi.org/10.1172/jci.insight.157342
60. Tamburin S, Mantovani E, De Bernardis E, et al (2021) COVID-19 and related symptoms in patients under disulfiram for alcohol use disorder. Intern Emerg Med 1–4.https://doi.org/10.1007/s11739-021-02633-y
61. Fillmore N, Bell S, Shen C et al (2021) Disulfiram use is associated with lower risk of COVID-19: a retrospective cohort study. PLoS One 16:1–9. https://doi.org/10.1371/journal.pone.0259061